Characterization of hierarchical structures in remelted Ni-Mn-Ga substrates for directed energy deposition manufacturing of single crystals

Tyler Paplham[a], Jakub Toman[a], Markus Chmielus[a]
[a]Department of Mechanical Engineering and Materials Science, University of Pittsburgh, Pittsburgh, PA 15261


Tyler Paplham

Tyler is a Materials Science and Engineering major from Buffalo, NY. He has worked in the Advanced Manufacturing and Magnetic Materials lab for nine months. After graduation, he plans to pursue his PhD in Materials Science and Engineering to research materials for sustainable energy generation and transmission.


Dr. Markus Chmielus

Dr. Markus Chmielus has been an Associate Professor in the Mechanical Engineering and Materials Science Department since 2013. He previously worked at Cornell University (postdoc) and the Helmholtz Center for Materials and Energy in Germany (research scientist), and has degrees from the Technical University of Berlin, Boise State University, and the University of Stuttgart in Materials Science and Aerospace Engineering. He now leads the Advanced Manufacturing and Magnetic Materials Laboratory (AM^3), where his group members perform experimental additive manufacturing and post-processing research on functional magnetic and structural metals.

Significance Statement

This work aims to provide a deeper understanding of how varying laser power and travel velocity affects the resolidification behavior in directed energy deposition, with a goal of successfully producing additively manufactured single crystals. Trends in properties of the remelted substrate as functions of each variable were suggested.

Category: Experimental research

Keywords: **Additive manufacturing, directed energy deposition, magnetic shape-memory alloys**

Abstract

Magnetic shape-memory alloys (MSMAs) such as Ni-Mn-Ga Heusler alloys have been of great interest in the past decade due to the observed inverse magnetoplastic (IMP) effect, wherein an applied mechanical stress reorients the direction of easy magnetization of the crystal. However, practically large strains achieved with this mechanism may only be generated from single crystals, the manufacturing of which is traditionally time-intensive and delicate. A possible approach for more quickly producing single crystal MSMAs is to use directed energy deposition (DED), a type of laser additive manufacturing. This study focused on the laser remelting of an austenitic $Ni_{51}Mn_{24.4}Ga_{24.6}$ single crystal substrate without deposition of an additional layer, so as to observe the effects of varying laser power and travel velocity on the resulting melt pool. Using digital microscopy and image analysis, various properties of the melt pool and contained microstructures were measured as functions of laser power and travel velocity. Some trends were suggested that provided insight into which parameter values are conducive to retention of a single crystal; however, a more comprehensive study is needed to confirm these trends.

1. Introduction

Magnetic shape-memory alloys are a unique class of metals which exhibit large reversible plastic deformations (up to 6-12% strain) upon a change of direction of easy magnetization in the crystal, which may be induced by a changing external magnetic field or an applied mechanical stress. This is made possible due to the presence of martensitic twin variants, which are alternating regions within the crystal structure with differing directions of easy magnetization. The lattices in each region are misaligned by almost ninety degrees, such that the twin boundary defines a dislocation line. Upon the application of an external magnetic field or mechanical stress, these boundaries “travel” throughout the crystal in a continuous series of dislocations, resulting in a macroscopic plastic deformation as the crystal structure transitions from one alignment to another [1,2].

These materials are of great interest due to their possible applications in powering sensors, actuators, and other small devices through the magnetic field induced strain and the IMP effect [2]. While the amount of power produced is small, MSMAs have notably high fatigue resistance and high energy density [3,4]. However, even this very small amount of power requires that the MSMA be a single crystal. Grain boundaries, inclusions and other dislocations introduce “pinning sites” which inhibit the motion of twin boundaries, limiting the magnetoplastic strain and thus the amount of power that can be produced. Single crystals are traditionally produced via Bridgman crystal growth, by which an ampule of molten metal is extremely slowly drawn across a very steep temperature gradient [5]. This is a time-intensive process that also leads to macrosegregation and thus inconsistency in composition across the crystal [6].

Additive manufacturing, specifically DED, may provide an avenue for more quickly producing single crystals with a lower level of macrosegregation. In this laser additive manufacturing method,

nozzles adjacent to the laser spray converging jets of metal powder into the laser beam, where it is melted along with the substrate surface to form a new layer of deposited material [7]. Before this method can be fully utilized in the printing of Ni-Mn-Ga single crystals, it must first be understood how the thermal history from the DED process affects the microstructures formed after remelting and deposition of a new layer. This experiment focused only on the remelting process, so as to determine individually the effect of varying the laser parameters on remelting of the original substrate without having to consider the complicating addition of a newly deposited layer of powder.

2. Materials and Methods

The substrate used was assumed to be an austenitic single crystal and had a nominal composition of $Ni_{51}Mn_{24.4}Ga_{24.6}$. An Optomec laser engineered net shaping (LENS) 450 system was used to remelt the substrate. For each track, the nominal laser power and travel velocity were chosen, then the laser was positioned and started a distance away from the substrate so that the full velocity had been reached by the time the laser made contact with the substrate. The laser was then shut off again a distance away from the substrate, then repositioned for the next track. Eight parallel tracks were made on the substrate surface. The substrate was then sectioned along a plane parallel to the top surface, revealing undisturbed material on which a ninth track (350-10) was made. The laser power and travel velocity were varied, and the chosen combinations are listed in Table 1. Each track was cut perpendicular to the travel velocity at approximately the halfway point in the track, mounted, polished, and etched to reveal the melt pool. The melt pools were then imaged on a digital microscope and analyzed in ImageJ.

Laser Power [W]	Velocity [mm/s]
100	0.5 1 2.5
200	2.5
250	1 2.5 5 10
350	10

Table 1: Laser power and travel velocity combinations for each track.

3. Results

Melt pools were observed in six of the tracks and are shown in Fig. 1. The remaining three tracks, all with a power of 100W, did not exhibit a melt pool and therefore are not shown.

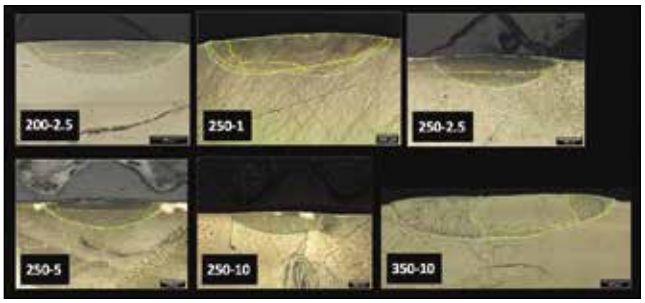

Figure 1: The six melt pools with parameters listed as power-velocity. The outline of each meltpool is shown in blue, while regions of different structure are outlined in yellow. All scale bars (lower right of each sub-image) read 200μm.

Of great importance to the determination of appropriate parameters for single crystal remelting and deposition are the nature of the hierarchical structures within the melt pool, namely the planar solidification region (PSR) and dendrites. The individual effects of laser power and laser travel velocity on the thickness of the PSR and the normalized depth of transition from [100] dendrites, oriented out of the page in Fig. 1, to [001] dendrites, oriented toward the top of the page in Fig. 1, are plotted in Fig. 2 and Fig. 3, respectively, where the normalized depth of transition is defined as the ratio of the depth of the [100] dendrites to the total depth of the melt pool.

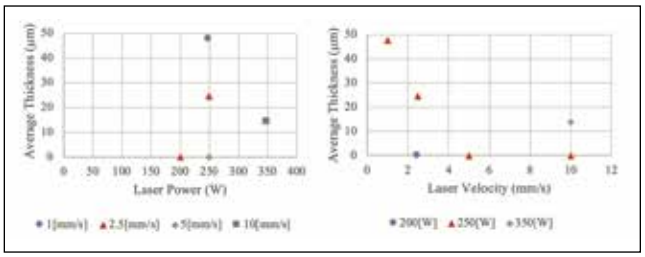

Figure 2: Thickness of planar solidification region (PSR) as a function of laser power (left) and laser travel velocity (right). Note that tracks which did not exhibit melt pools are excluded.

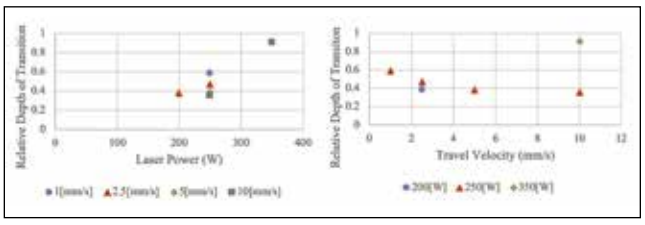

Figure 3: Relative depth of transition from [100] dendrites to [001] dendrites as a function of laser power (left) and laser travel velocity (right). As before, tracks which did not exhibit melt pools are excluded.

The thickness of the PSR appeared to increase with increasing laser power and decreasing travel velocity. However, there seems to be some minimum power or maximum travel velocity required for formation of the PSR, as the 200-2.5, 250-5, and 250-10 tracks did not have observable PSFs, suggesting that a threshold value for formation lies in the range of 200-250W and 2.5-5mm/s for varying laser power and travel velocity respectively. The relative depth of transition from [100] dendrites to [001] dendrites also increased with increasing power and decreasing velocity.

A qualitative analysis was also performed on the observed dendrite angles. Dendrite regions, defined by the yellow subdivisions in Fig. 1, were characterized as vertical, diagonal, horizontal (all within the plane of the page), or [100] (out of the page). The melt pools were assumed to be sufficiently symmetric that no insight was lost by combining the right and left diagonal or horizontal (or vertical in the case of 250-1) groups into merely "diagonal" or "horizontal" (or "vertical"). The percentages of each type of dendrite orientation for the 250W melt pools are plotted in Fig. 4, which shows the effect of varying laser travel velocity on dendrite orientations with power held constant. A similar plot of the 2.5mm/s melt pools at 200W and 250W is also shown in Fig. 4, although this is less enlightening because only two tracks were created at the same velocity (at least out of those which resulted in melt pools).

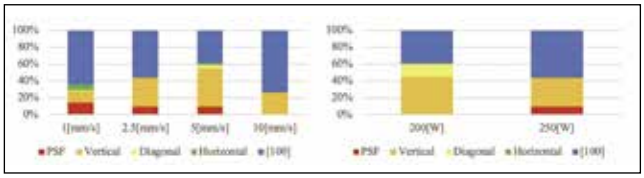

Figure 4: Percentages of various dendrite orientations at constant power of 250W (top) and constant travel velocity of 2.5mm/s (bottom).

It is difficult to discern any conclusion from Fig. 4 other than the behavior of the planar solidification front, which was already shown in Fig. 2. It is interesting that 250-1 and 250-5 exhibit diagonal and horizontal dendrite groups but 250-2.5 does not.

4. Discussion

The trends shown in Fig. 2-3 are consistent with expected resolidification behavior. As a crystal solidifies, the solidification front is initially planar, as this results in equal surface energy across the entire front. However, protruding points caused by thermodynamic variation along the surface will be supported by constitutional undercooling present ahead of the interface. Thus, the planar front breaks down. Solidification tends to be more energetically favorable along the crystal lattice axes (usually defined along <100>), resulting in pointed structures called dendrites along the lattice axes. Varying the laser power and travel velocity alters melt pool shape, thermal gradient, velocity of the solidification front, etc. These parameters drive transition from planar to dendritic fronts and the selection of dendrite growth axis.

A satisfactory albeit simplified explanation for the trend in relative depth of the [100] to [001] transition concerns how adjusting the laser parameters affects the shape of the melt pool. High power and low velocity result in a deep, abrupt melt pool whereas low power and high velocity result in shallower, more gradual melt pools. The solidification front advances with a velocity normal to itself, but the allowable directions of dendrite growth are limited to <100>. The dendrite growth must keep up with the solidification front, so the direction selected will be that which requires the lowest growth rate for the dendrites. As can be seen in Fig. 5, an abrupt, deep melt pool such as in the (250-1) and (350-10) tracks will have more dendrite growth in the [100] direction, whereas a shallow, gradual melt pool such as in (250-2.5) and (250-5) will have more dendrite growth in the [001] direction. If a deep melt pool and shallow melt pool are sectioned at approximately the same distance along the track, this manifests as the deep melt pool showing a greater presence of [001] than shown by the shallow melt pool [8].

The behavior of the PSR is also complex. A high thermal gradient promotes planar growth, as thermal effects dominate over other influences and thus best preserves a quasi-steady state environment. According to the thermal model used in Gäumann et al., the Rosenthal solution predicts that the average of the ratio $G^{3.4}/V$ decreases with increasing power, where G is the thermal gradient and V is the velocity of the solidification front. This is in disagreement with what was observed in the present study, where planar growth increased with increasing power. However, it is crucial to note that the Rosenthal solution predicts that the *average* $G^{3.4}/V$ decreases with increasing power. The value of $G^{3.4}/V$ is very high at the beginning of solidification, but then decreases rapidly at a slowing rate with increasing z, where z is the depth from the surface of the melt pool (i.e. any point in the melt pool has a negative z-value) [9]. It is hypothesized that perhaps increasing the power results in a slower initial rate of decreasing $G^{3.4}/V$. Because of the shape of the curve, this could result in maintaining a thermal gradient sufficient for planar growth across a greater range of z while still showing a lower overall average value.

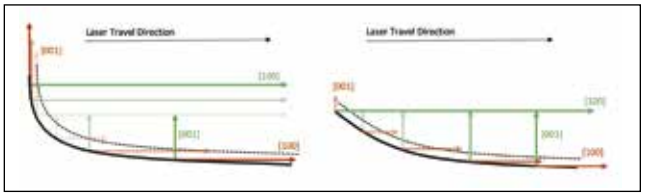

Figure 5: Schematic of preferred dendrite growth directions in deep, abrupt melt pools (left) and gradual shallow melt pools (right). Direction of easy growth, i.e. the observed growth direction, is shown in green, while the rejected direction is shown in red. The [010] direction has been omitted for simplicity.

5. Conclusion

Overall, the effects of varying laser power and travel velocity on many properties of the melt pools and their contained structures were able to be analyzed either quantitatively or qualitatively. Some trends were implied, many of which agreed with prediction. However, due to the small amount of available substrate and therefore the low number of samples, such trends would be highly vulnerable to any outliers or errors in measurement and are thus not reliable. A more comprehensive study in which either laser power or travel velocity in smaller increments should be performed to confirm the suggested trends. Additionally, since the overall goal of this project is to print single crystals with DED, a similar study should be conducted with samples that were remelted *and* had an additional layer of powder deposited.

6. Acknowledgements

This project was funded by NSF grant #1808082 including an REU supplement and the Mascaro Center for Sustainable Innovation. Additionally, the authors would like to thank all colleagues in the Advanced Manufacturing and Magnetic Materials lab for support during this project.

7. References

[1] Chmielus, M. (2010) “Composition, structure and magnetomechanical properties of NiMn-Ga magnetic shape-memory alloys.” Logos Verlag Berlin.

[2] Carpenter, D. (2008) “The application of ferromagnetic shape memory alloys in power generation devices”. Boise State Uni. Th. And Diss. 544

[3] Chernenko, V. A. et al. (2009) “Large magnetic-field-induced strains in Ni-Mn-Ga nonmodulated martensite”. Appl. Phys. Lett. 95

[4] Rizzello, G. et al. (2017) “An overview on innovative mechatronic actuators based on smart materials”. IEEE Africon 2017 (pp. 450-455)

[5] Hage-Ali, M. & Siffert, P. (1995) Growth Methods of CdTe Nuclear Detector Materials. In T. D. Schlesinger, R. B. James (Eds.) Semiconductors and Semimetals (pp. 219-255)

[6] Boonyongmaneerat, Y. et al. (2007) “Increasing magnetoplasticity in polycrystalline NiMn-Ga by reducing internal constraints through porosity”. Phys. Rev. Lett. 99

[7] Liu, D. et al. (2014) “Laser engineered net shape (LENS) technology for the repair of Nibase superalloy turbine components”. Metall. Mat. Trans. A 45 (pp. 4454-4469)

[8] Rappaz et al. (1989) “Development of microstructures in Fe-15Ni-15Cr single crystal electron beam welds”. Metall. Mat. Trans. A 20A (pp. 1125-1138)

[9] Gaümann, M. et al. (2001) “Single-crystal laser deposition of superalloys: processing microstructure map”. Acta Materialia 49 (pp. 1051-1062)